The ν-ball γ-spectrometer

M. Lebois, N. Jovančević, D. Thisse, R. Canavan, D. Etasse, M. Rudigier, J.N. Wilson

Nuclear Inst. and Methods in Physics Research, A 960 (2020) 163580

Contents lists available at ScienceDirect

Nuclear Inst. and Methods in Physics Research, A

journal homepage: www.elsevier.com/locate/nima

The ν-ball γ-spectrometer

M. Lebois [a,b,*], N. Jovančević [a], D. Thisse [a], R. Canavan [c,d], D. Étasse [e], M. Rudigier [c], J.N. Wilson [a]

[a] Université Paris-Saclay, CNRS/IN2P3, IJCLab, 91405 Orsay, France
[b] Institut Universitaire de France, 1 Rue Descartes, 75005 Paris, France
[c] Department of Physics, University of Surrey, Guildford, GU2 7XH, UK
[d] National Physical Laboratory, Teddington, UK
[e] Laboratoire de Physique Corpusculaire, Caen, France

ARTICLE INFO

Keywords:
γ-spectrometer
HPGe
$LaBr_3$
FASTER
Hybrid array
ALTO
LICORNE
Fast neutrons induced reactions

ABSTRACT

The ν-ballspectrometer is an hybrid array combining high purity co-axial germanium detectors from the french-UK loan pool, clover detectors from the GAMMAPOOL, lanthanum bromide ($LaBr_3$:Ce) scintillator detectors belonging to the FATIMA collaboration and phoswitches from the PARIS collaboration. The aim was to couple the excellent energy resolution of germanium detectors to the excellent time resolution of the $LaBr_3$ detectors. We achieved a total photopeak efficiency of 6.7% at 1.3 MeV, and peak-to-total ratio of 50% for the germanium part of the array. Using the digital acquisition system FASTER, we achieved time resolution of about 250 ps for $LaBr_3$. This acquisition system made also possible the use of the calorimetry for reaction selection. It makes ν-ball the first fully digital large fast timing spectrometer with time resolution similar to analogue electronics. The construction began in June 2017 and commissioning was performed in early November 2017. From November 2017 to June 2018, more than 3200 h of beam time were provided by the ALTO facility to perform eight experiments during the campaign. Among them, five weeks of beam time were dedicated to γ spectroscopy of fast neutron induced reactions. In this paper all the technical details about the spectrometer are presented. First steps of the data analysis process are also discussed.

1. Introduction

Gamma ray spectroscopy is a tool used in nuclear physics research which has permitted the gathering of great quantities of information about excited nuclear states over previous decades. With the development of high efficiency Germanium spectrometers such as EUROGAM, EUROBALL and GAMMASPHERE [1–4], highly detailed coincidence spectroscopy has been performed over a wide range of atomic nuclei, allowing detection of γ transitions as weak as 10^{-5} [1–4] of the total reaction cross section. Information on spins and parities of these excited states can also be deduced with pure Germanium detector arrays using measurement techniques such as γ-rays angular distributions, angular correlations and polarizations. However, to obtain information on nuclear lifetimes, and hence nuclear moments, it may require Germanium arrays to be coupled to ancillary devices such as plungers — to measure lifetimes in the 1–100 ps range [5,6]. Over the last decade, new types of fast-scintillator such as $LaBr_3$ have become available [7]. The use of these crystals as scintillator detectors allows the access to lifetime information in the 10 ps to 10 ns range. The possibility of an hybrid spectrometer combining both types of detector (Ge for energy selectivity and $LaBr_3$ for fast timing [8]), such as the ROSPHERE array [9], has thus recently been opened.

In this context we developed the ν-ball spectrometer at the ALTO facility of the IPN Orsay in order to push the hybrid concept further. The ALTO facility also offers the possibility to use such a hybrid spectrometer to study excited states and lifetimes in very neutron-rich nuclei [10–12] by inducing fission of $^{238}_{92}$U or $^{232}_{90}$Th in the center of the array with the LICORNE directional fast-neutron beam [13]. In addition, the 15 MV Tandem Van de Graaff accelerator also produces a wide range of stable beams with an excellent time structure (2 ns pulse width with a repetition period of 400 ns), thanks to the beam buncher. In this paper we describe the technical aspects and innovations of the ν-ball device, which include a fully digital data acquisition (DAQ), and the capability of simultaneously performing Compton suppression and reaction calorimetry using BGO shields. Some aspects of data analysis procedures will also be discussed.

2. Presentation of the ν-ball spectrometer

The ν-ball array combines 24 Ge clovers from the GAMMAPOOL [14], 10 co-axial high purity germanium (HPGe) detectors and 20 $LaBr_3$ or 34 PARIS phoswiches detectors [15–17]. Fig. 1 shows a photo

* Correspondence to: Laboratoire de Physique des 2 Infinis Irène Joliot-Curie, UMR 9012 CNRS/In2p3, Université Paris-Saclay, Site Orsay Bâtiment 100 et 200, 91898 Orsay Cedex, France.
E-mail address: lebois@ipno.in2p3.fr (M. Lebois).

https://doi.org/10.1016/j.nima.2020.163580
Received 18 July 2019; Received in revised form 28 January 2020; Accepted 1 February 2020
Available online 5 February 2020
0168-9002/

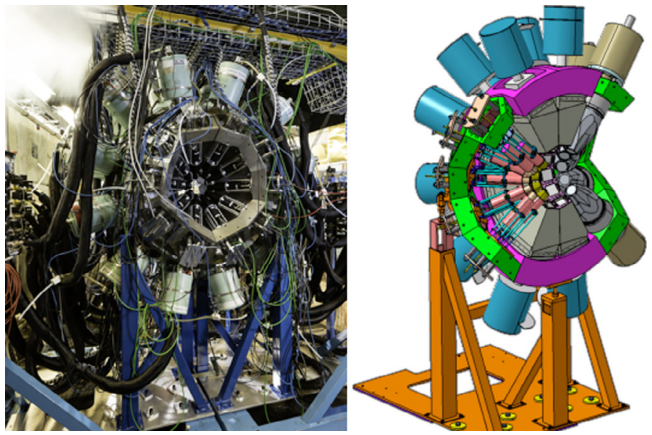

Fig. 1. Photograph of the ν-ball array installed in the experimental area of the ALTO facility (left panel) and a technical drawing of one ν-ball hemisphere (right panel).

of the array (on the left). On the right a technical drawing shows the three types of detector: HPGe clover detectors and their associated Compton shield (the two central rings), co-axial HPGe detectors (right ring) and $LaBr_3$ in the left ring.

Three main characteristics for the ν-ball concept need to be optimized to ensure maximum performance:

- Use of Compton shields to reduce Compton background and increase photopeak visibility in gamma spectra. Furthermore, the absence of heavy metal collimators on the BGO detectors will allow these detectors to function simultaneously as a Compton rejection tool and contribute to the event-by-event calorimetry of the nuclear reactions studied.
- Inclusion of $LaBr_3$ detectors to facilitate measurements of excited nuclear states lifetimes in the 10 ps–10 ns range.
- Use of a fully digital DAQ system to allow processing of very high count rates, to minimize the dead time, optimize the time resolution of all the different detector types, and to make the signal processing simpler. Such a system can be run in either triggerless or triggered mode.

Several GEANT4 [18] simulations were performed to optimize the geometry of the array. The final configuration of the spectrometer is presented in Fig. 1. Since the spectrometer is intended to often be used with neutron beams no detectors are placed at forward angles (<20 degrees) to allow neutrons to escape the array without touching a detector — and potentially damage it. The $LaBr_3$ are preferentially placed as two forward rings since they are much more resilient to scattered neutrons.

2.1. Description of ν-ball components

2.1.1. The co-axial high purity germanium detectors

Ten coaxial Germanium detectors, named "Phase I", were placed in a ring at backward angles (133.5° with respect to the beam axis) and 16 cm from the center of the sphere to the BGO shield entrance window. That sets the crystal at 18 cm from the center. They were rented to the FRENCH/UK loan pool [19] for the duration of the campaign. These detectors are of n-type hyper pure germanium detectors from the EUROGAM collaboration [1]. HPGe crystals are tapered over the front 30 mm of their length to allow for closer packing when in the array. The detectors have a typical energy resolution of 2.5 keV (for 1.33 MeV γ-rays) and a relative efficiency of 75% [1].

These germanium detectors are surrounded by BGO escape suppression shields which are divided into ten optically isolated crystals, each coupled to a photomultiplier (PM) readout. Each of these has a resolution of 18–22% at 662 keV when the source is placed at the germanium crystal position. The PM tubes are gain matched and daisy-chained with 0.5 ns LEMO cables to obtain a single summed output signal per shield which is fed directly into the digitizer without pre-amplification. This will allow a approximated measurement of the energy deposited in the BGO shield.

2.1.2. The clover high purity germanium detectors

The clover Germanium detectors were borrowed from the GAMMAPOOL [14] for the duration of the campaign and are placed in two rings of twelve detectors each around 90° (75.5° and 104.5° with respect to the beam axis) to take advantage of their granularity in case of Doppler corrections. The distance from the BGO shield entry to the center was 17 cm which places the crystals at 24 cm from center. Each detector consists of four germanium crystals of 50 mm diameter and 70 mm height packed in a close geometry. After add-back, these have a very high total efficiency ($\epsilon \sim 130\%$), among the world's largest for N-type Ge detectors. Each clover detector is surrounded by its own BGO anti-Compton shield. These are divided into sixteen optically isolated crystals, each with a photomultiplier readout. The signals from the PM tubes are daisy-chained into two groups of eight to obtain two signals per anti-Compton shield and are directly digitized without preamplification. Again this will allow the use of BGO shield for energy measurement at the same time as Compton rejection.

2.1.3. The $LaBr_3$:Ce detectors

To add fast-timing capabilities and complete the array, twenty $LaBr_3$:Ce crystals, on loan from the FATIMA [20] and UKNDN [21] collaborations were used. The remaining ten percent of available solid angle in the sphere permitted the packing of 20 of these detectors in two rings of ten. The first ring was 46.5° with respect to beam axis and 11 cm away from the sphere center. The second ring was 34° with respect to beam axis and 15 cm away from the sphere center. When coupled to the LICORNE directional neutrons source, the ν-ball $LaBr_3$ second ring had to be moved further away from the center (~25 cm) in order to be outside the neutron cone. Two types of $LaBr_3$ detector were used:

- $1.5'' \times 2''$ cylindrical crystals coupled to Hamamatsu R9779 photomultipliers tubes (PMT). These detectors can achieve an energy resolution of ~ 3% at 662 keV and a coincidence resolving time of 210 ps at 1332 keV. This later value was measured as the Full Width Half-Maximum (FWHM) of the time distribution of the coincidence between full energy peaks of the $^{60}_{27}$Co source.
- $1'' \times 1.5'' \times 2''$ conical crystals coupled to Hamamatsu R9779 PMTs. These detectors can achieve a coincidence resolving time of 160 ps at 1332 keV and have a slightly better energy resolution (~ 2.7% at 662 keV) than the cylindrical ones.

The reference layout of the array is presented in Fig. 1. A technical drawing from the IPNO design office of one hemisphere is presented in the right panel. Two rings of $LaBr_3$, two rings of clovers embedded in their BGO shields and a last ring of Phase I detectors in their shields are visible from left to right. The left panel shows a photograph of the array at the beginning of the experimental campaign before the mounting of the reaction chamber.

A separate configuration involving the coupling of ν-ball with four clusters of the PARIS [15–17] array was also performed. For this setup all the $LaBr_3$ detectors were replaced by 34 PARIS phoswitches almost completely covering the available solid angle in the forward direction (~ 30%). Each PARIS phoswich consists of a $LaBr_3$:Ce crystal optically coupled to a NaI(Tl) crystal. The inner shell is $LaBr_3$:Ce cubic crystals ($2'' \times 2'' \times 2''$) and the outer shell consists of NaI(Tl) rectangular crystals ($2'' \times 2'' \times 6''$). Both crystals are encapsulated in an Aluminum can, sharing one common photomultiplier tube. Because of the decay time difference in each crystal, pulse shape discrimination can be applied to distinguish the energy deposited in each layer. With this technique, the phoswitches still benefit from the better energy and time

resolution of the $LaBr_3$ layer. The NaI layer is mainly used to increase the high energy γ detection efficiency — up to 40 MeV nominally. An optimal time resolution of $\sim$ 450 ps could be achieved for these detectors using a $^{60}_{27}$Co γ source.

2.2. The data acquisition system: FASTER

All the pre-amplifier or anode signals are sent to a fully digital acquisition system called FASTER (Fast Acquisition System for nuclEar Research) [22] developed at the Laboratoire de Physique Corpusculaire in Caen France. It is used to measure relevant observables (deposited energy and time of each hit) extracted online from the traces. FASTER has been built to be modular and fully integrated to satisfy the needs of any type of experiment in nuclear physics, particularly those which combine detector types with significantly different characteristics. FASTER is capable of on-line processing of traces, to sort them and group them into "events" (depending on each experiment scientific goal) through a software event builder module, no matter what is the type of detector. At the same time, data can be visualized using the versatile ROOT Histogram Builder (RHB) software. Based on ROOT [23], it allows the implementation of online energy, time-of-flight (TOF) spectra or any kind of 1D-2D user-defined histograms. The FASTER system is based on two different types of cards that can be connected to a single motherboard:

- CARAS daughterboard. The main feature of this card is a 500 Msp/s 12 bits digitizer which discretize the incoming pre-amplifier signal. Then different algorithms which mimic the operations performed by an ADC, QDC or TDC can be uploaded on an embarked FPGA processor. In the context of ν-ball, these cards are used to process the scintillators signals. For the $LaBr_3$ signals, the QDC algorithm is used. It features a digital constant fraction discriminator mode with zero-crossing interpolation, providing the best time resolution. The BGO uses an ADC integrator-differentiator algorithm called CR-RC4 which provides the best results for Compton suppression and gives the best information on the deposited energy. The CARAS cards also possess a "RF" module which digitizes the high frequency (2.5 MHz) signal of the beam pulsation and produces time stamps corresponding to one beam pulse in every thousand and sends them to the data stream. As the period is measured with a ps precision, every beam pulse time stamp can be precisely reconstructed offline during the data analysis process. This provides a precise reference clock for an entire measurement.
- MOSAHR daughterboard. The main feature of this card is a 125 Msp/s 14 bits digitizer which processes the incoming pre-amplifier signal. The FPGA can accept only an ADC algorithm such as CR-RC4 or trapezoidal to calculate the amplitude and time stamp of each hit. All the germanium crystals signals are sent to these MOSAHR daughterboards. To minimize low-energy walk and get the best timing properties for ν-ball, the trapezoidal filter was selected since it is using a constant fraction discrimination module instead of a leading edge discriminator module.

All the signals of the ν-ball array are sent to 184 (200 with the PARIS setup) independent electronics channels. These are distributed over 34 motherboards in three μTCA crates. The crates are synchronized using an external logic signal (called "t0") distributed by a MCH card located in a fourth crate. The data acquisition can be run in two modes: setup or disk mode. In the setup mode, the standard FASTER graphical user interface can be used to change tuning parameters, implement a trigger condition or visualize online spectra. The disk mode skips the graphical part and takes the data sent by each motherboard and writes it to a data server. The 34 data streams are merged offline to form a unique time sorted 30 s long data file that is directly usable. Transfer rates, from the crates to main operating computer of about 70 Mb/s were achieved with a writing to disk rate ranging from 5 Gb/h to 100 Gb/h max, depending on the trigger conditions. This limitation was corresponding to the maximum transfer rate implied by the use of two coupled 1 Gb optic fibers for the network connection between crates and server. The maximum corresponding count rates, obtained during the campaign, in the individual detectors are : 10 kHz for the HPGe, 15 kHz for the $LaBr_3$ and 40 kHz for the BGO crystals.

2.3. ν-ball as a calorimeter

The full digitization of the ν-ball array, and the capacity to process very high count rates in the detectors with no significant dead time, opens up the possibility of performing reaction calorimetry; The array operates in a mode where measurements of γ-ray multiplicity, M_γ (referred as k), and total energy deposited in the array, E_{tot} (referred as H), are made for each event detected.

For ν-ball to perform simultaneously as a Ge high-resolution spectrometer and a calorimeter requires the heavy metal collimators, that normally shield the front faces of the BGO anti-Compton detectors from direct hits, to be removed. Each BGO unit then simultaneously operates to detect and veto γ-rays which scatter out of the Germanium crystals (indirect hits), and to detect gamma rays which only hit the BGO (direct hits).

Calorimeters were a feature of early γ-ray spectrometers [24–26] and offered two major advantages: firstly, a significant gain in selectivity due to the ability to preferentially select different reaction channels of interest, and secondly the ability to measure multiplicity and sum-energy distributions for a given channel, which can be used to learn about the physics of a nuclear reaction and in particular its influence on angular momentum and energetics.

With ν-ball these calorimetry features/advantages are retained by making the BGO anti-Compton detectors dual-purpose. However, the benefit of significantly increased selectivity comes with associated array performance changes and some minor costs:

i. A slight decrease in peak-to-total ratio (P/T), defined as (for mono-energetic γ-ray sources) the ratio of the integral of a photopeak and the total spectrum, and slight increase in Ge photopeak efficiency. The collimators normally shadow the edge of the Ge crystals forcing detected hits to be away from the crystal edge and nearer the center. The P/T ratio from both source measurements and GEANT4 simulations is shown to decrease from 50% with collimators to 40% without.
ii. False vetos. Two separate γ-rays hit the Ge and BGO crystals of the same detector module. The full energy photopeak of the γ-ray detected in the Ge will be vetoed, when in fact it ought not to be, and would not have been if the heavy metal absorber was in place. The loss in Ge photopeak efficiency for ν-ball is strongly multiplicity-dependent. At multiplicity 1 there is obviously no loss in performance at all. At multiplicity 30 the loss in Ge photopeak efficiency is expected to be greater than 10%. However, major physics motivations for constructing ν-ball were the study of neutron-induced fission and spectroscopy of two-neutron transfer reactions, both of which have a relatively low average spin and thus reasonable multiplicity. For the ^{238}U(n,f) reaction, the false veto rate was measured from the integral of residual photopeaks observed in the vetoed Ge-BGO coincidence spectra compared to those in the unvetoed Ge spectrum. The loss in photopeak efficiency was less than 3 percent for this reaction with an average multiplicity of approximately 7. Over the campaign, fission process is the reaction with the highest average γ multiplicity.
iii. An increase of a factor of 3–4 of BGO detectors count rate. At the very highest count rates, loss of efficiency may occur due to γ-ray pile-up effects. The BGO shaping time for ν-ball in the FPGA algorithms was 2 μs, and thus pile-up effects may start to become significant at rates of 20 kHz or more (an average time of 50 μs between two successive BGO hits).

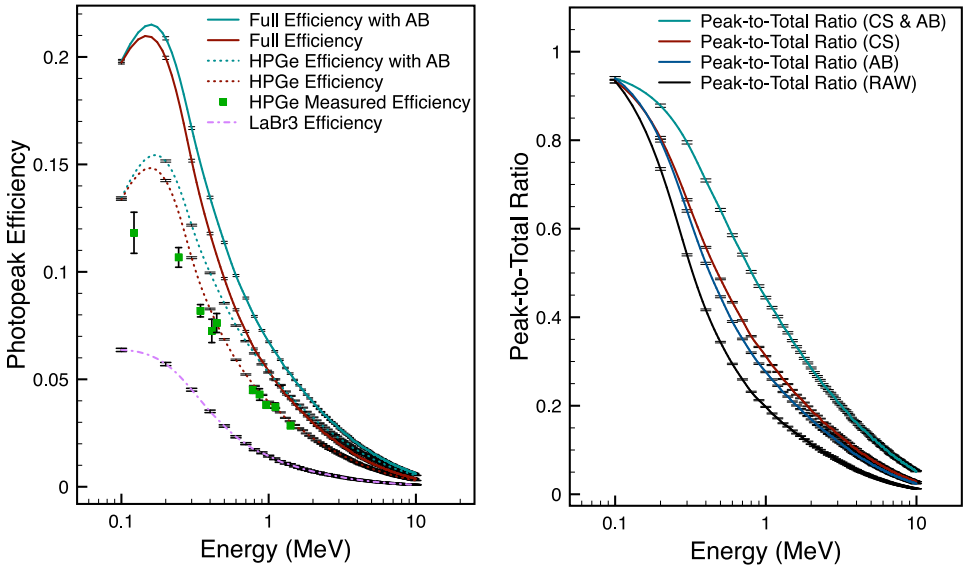

Fig. 2. On the left, the plot presents the photopeak efficiency of the ν-ball array. The lines are simulated results produced with GEANT4. The square are measured values for HPGe detectors only. On the right is presented the peak-to-total ratio as a function of the incident γ energy. The different curves shows the influence of Compton suppression using the BGO shields and/or the add-back procedure. Only statistical errors are shown for the simulation. More details are given in the text.

At maximum count rates, the ν-ball DAQ is capable of handling individual crystal hits at a rate of 3 MHz. This would correspond to the 106 Ge crystals each typically counting individually at 10 kHz and the 48 BGO channels each counting individually at 40 kHz. The ν-ball calorimeter performance is characterized by a total solid angle coverage of approximately 75% by active detectors. Typically the hits are recorded with proportions 75%, 20% and 5% in the BGO, Ge and $LaBr_3$ respectively. Based on a $^{60}_{27}$Co source measurement, the calorimetry total energy efficiency is 68%. The total photopeak efficiency is 48%. These values have been measured by conditioning in energy one reference detector and calculating the probability that another γ-ray is detected in the spectrometer. More precisely, the calorimetry efficiency is calculated by placing an energy condition (1332.5 keV) on the reference $LaBr_3$ and integrating the 1173.2 keV photopeak of all the other detectors. Studying the calorimetry of a given reaction (e.g. fission) requires an unfolding of the calorimeter response in two-dimensions to deduce the emitted total-energy and multiplicity distributions from the detected distributions [27].

2.4. ν-ball performance

2.4.1. GEANT4 simulations results

During the design process, Monte-Carlo simulations, using GEANT4, were performed to evaluate the characteristics of different considered geometries. The first goal was to maximize detection efficiency for Germanium and $LaBr_3$ parts of the array. After this first step, a mechanical study was performed to use and reinforce the preexisting mechanical base to hold the entire structure with supports from below, while preserving the possibility to move the two hemispheres apart to allow access to the reaction chamber or neutron source. The total weight of the detectors, full liquid nitrogen dewars and mechanical structure was 2.6 tons. A new simulation, using the final geometry, was then carried out to evaluate the performance of Compton suppression and add-Back and to obtain information on the photopeak efficiency and the peak-to-total ratio.

The results are represented by the curves shown in Fig. 2. On the left, the photopeak efficiency (calculated as the ratio of the number of counts in the full energy peak to the total number of emitted γ-rays) is plotted. The continuous lines take all the detectors (HPGe and $LaBr_3$) into account. The dashed lines represent only the germanium detectors. For both cases, two curves with or without add-back reconstruction in the clover detectors are presented. In these simulations, a simple add-back algorithm was used: the four crystals are considered as one. This algorithm is sufficient as one γ-ray is fired at once in ν-ball since the chances to have simultaneously three individual crystals fired in the same clover is negligible. As expected, the efficiency is slightly better with the second option as the procedure takes two counts from Compton plateau and generate a new count at the full-energy peak. A photopeak efficiency of 6.7% at 1.3 MeV could be achieved in an optimal geometry. The $LaBr_3$ component has been extracted from the total photopeak efficiency and is represented by the dot-dashed line. $LaBr_3$ participate up to 1.4% of the total photopeak efficiency at 1 MeV.

On the right side of Fig. 2, the evolution of peak-to-total ratio is plotted. This value is calculated as the integral of the full energy peak divided by the total integral of the spectrum. The dependance of this experimental parameter as a function of incident γ energy has been evaluated. Again, several cases were considered depending on the use of add-back and Compton suppression achieve an optimal 44% peak-to-total ratio at 1 MeV.

2.4.2. The measured energy performances

To validate the simulation results, calibration measurements using $^{152}_{63}$Eu and $^{60}_{27}$Co standard γ sources were performed. Fig. 3 shows that the energy resolution obtained for the sum of the 106 calibrated germanium channels is 2.35 keV with single detector resolution ranging from 1.7 keV for the best clover crystals to 2.9 keV for some of the larger phase I crystals. A similar spectrum for a $LaBr_3$ detector is given as an example. The measured resolution for this specific detector was 3.2% at 661.7 keV. This value is very representative of the cylindrical crystals. However, the conical shaped detectors have on average a better energy resolution of 2.7%.

In the campaign (detailed in Section 3), the geometry of the fast timing part of the array was frequently modified to satisfy the need for coupling to the LICORNE neutron source or to the PARIS array. Validation of the results obtained with the GEANT4 simulations was therefore only performed using the Phase I and Clover detectors with a fixed geometrical position. Using the energy spectrum in Fig. 3, the photopeak efficiency has been measured for an energy range of 121 keV to 1408 keV. The results are represented by the squares on the left plot in Fig. 2. One can see the excellent agreement between the simulation and the measurement for energies above 344 keV. The difference below is explained by the presence of some shadowing

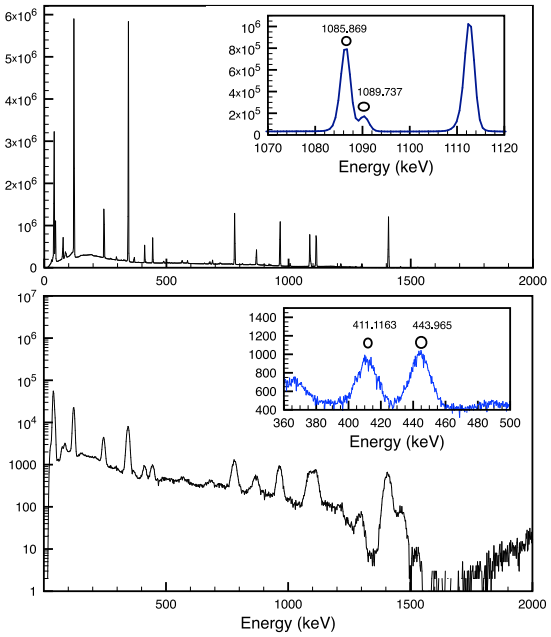

Fig. 3. On the top, cumulated HPGe spectra for a one hour data acquisition with $^{152}_{63}$Eu γ source. The subview is a zoom of the 1085–89 keV doublet to illustrate the energy resolution performances (2.35 keV at 1 MeV). The lower picture is an energy spectrum measured with a cylindrical $LaBr_3$. The subview is a zoom on the 411 and 443 keV gamma lines to demonstrate the energy resolution measured with these scintillator (3% at this energy).

effects from the LICORNE reaction chamber (∼ 2 cm total thickness of aluminum) that partially shadowed Phase I detectors and therefore decreased their efficiency in the lower energies region — see Fig. 5. The peak-to-total ratio has been measured using a $^{137}_{55}$Cs source. Due to the small activity (40 kBq) and small γ multiplicity of this source, it was the most likely to reproduce the GEANT4 results that were simulating mono-energetic sources. A value of 50% has been measured when using the same simple add-back algorithm (as in GEANT4 simulation) and Compton suppression. This is close to the 55% value from the simulations. However, depending on the experiment performed, more specifically on the count rates and typical multiplicities observed, a careful study of an adequate add-back algorithm will be needed. As a consequence, lower performances might be obtained.

2.4.3. The measured timing performances

In every experiment of the campaign, the beam was pulsed with a period of 400 ns and a pulse width of approximately 2 ns. Some of the beam pulses of the RF signal were written in the data stream (*cf.* Section 2.2). Nonetheless, a sub nano-second timing resolution can be achieved with the $LaBr_3$ crystals mounted in the array. To evaluate the time resolution of the different components of ν-ball a one hour measurement with a $^{60}_{27}$Co source has been performed. Then, the time difference distribution between a reference detector (energy conditioned by the 1132.5 keV γ) and another detector (energy conditioned by the 1173.2 keV γ) were reconstructed and the time difference spectrum of each pair of detectors was implemented. The FWHM of these time distributions was automatically measured using a gaussian fit. From these, the detector that systematically gave the smallest FWHM (a conical $LaBr_3$ with label 210) was selected to be the reference detector for timing measurement.

In Fig. 4, the time difference spectrum of five different detectors with respect to the reference $LaBr_3$ are shown. One can notice the small FWHM of the $LaBr_3$/$LaBr_3$ time distributions of about 200 ps. This value is compatible with the intrinsic timing resolution of the FATIMA collaboration cylindrical crystals. The nominal timing resolution (150 ps)

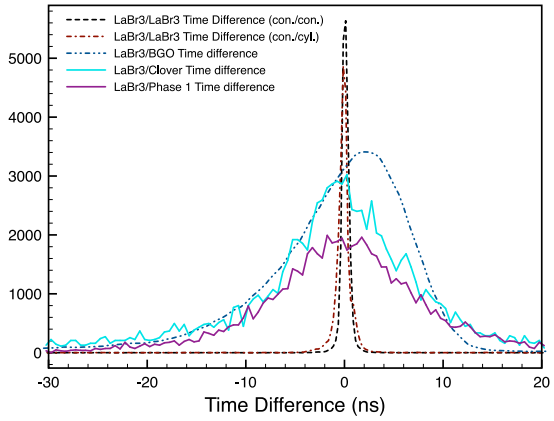

Fig. 4. Energy conditioned time spectra between two detectors. It represents the time difference between a reference $LaBr_3$ (conical) conditioned on the 1332.5 keV γ of $^{60}_{27}$Co with other detectors: $LaBr_3$ (cylindrical or conical), Phase I and Clover crystals, BGO crystal. The second detector was conditioned on the 1173.2 keV γ ray. In the legend, con. stands for conical and cyl. stands for cylindrical.

for the conical shaped scintillators could not be reached, presumably because of the limitations of the 500 MHz sampling frequency of the digitizers. Indeed, the short rise time of the signal (∼ 2 ns) is the same as the sampling period. As a consequence, the zero-crossing, with the CFD algorithm implemented in FASTER, had to be performed on the decay part of their signal hence decreasing the effective time resolution.

In Fig. 4, the scattering curves corresponds to HPGe measurements. The average time resolution obtained is about 13 ns, which is very close to the intrinsic value of approximately 10 ns. The smoothed (for readability) curve is a time spectrum for a BGO crystal. The measured time resolution (∼ 15 ns) is not typical of what can be obtained with a scintillation detector under the best conditions. Scintillators usually have better time resolution than semi-conductor detectors. However, as the BGO will mainly be used for Compton suppression, *i.e.* in coincidence with HPGe, 15 ns was considered as a reasonable value. In conclusion, the ν-ball array measured performances correspond to the expected ones. Furthermore, a fully modular GEANT4 geometry has been implemented that provides an excellent reference tool to calculate response functions and support data analysis.

3. The ν-ball campaign

The ν-ball spectrometer was operational over a one year period from November 2017 to June 2018. Over 150 researchers participated in the experimental campaign and approximately 3200 h of beam time were provided by the ALTO facility. A detailed description of the campaign progress is given in [28]. Eight experiments were performed, a short description of some of them is given in [10–12]. The variety of physics cases necessitated several transformations of the geometry during the course of the campaign.

After construction a commissioning experiment was performed using an ionization chamber with a Frisch grid containing a ^{252}Cf spontaneous fission source of 3 kBq on a lead backing at the central cathode to stop one of the fission fragments. The chamber of 15 cm diameter was placed in the center of the array and the ν-ball data acquisition triggered with the chamber cathode signal. The test was used to validate the DAQ system at a low count rate with fission events of an average gamma multiplicity around 8. Data were acquired for around 50 h.

Subsequently a first set of experiments [10,11] based on heavy-ion fusion-evaporation reactions were performed with all ν-ball detectors placed in the most compact geometry possible — identical to the previously simulated GEANT4 setup. The trigger condition was multiplicity of two γ rays detected in any $LaBr_3$ module (or one Ge module and

Fig. 5. The top panel shows a photograph of the experimental setup of ν-ball coupled to the PARIS array. The bottom panel shows the ν-ball array coupled to the LICORNE neutron production chamber.

one $LaBr_3$) within 2 μs. Clover modules had a local trigger on the card, to provide a multiplicity of one, even in the event of more than one clover crystal firing.

Later experiments required a change in geometry to couple the array with the LICORNE neutron source [12]. The neutron source produces naturally directional neutrons in a cone that depends on the primary beam energy.

The presence of the LICORNE chamber and the heavy metal collimator, that shield the gas cell, causes a partial shadowing effect on the backward ring of coaxial germanium detectors, thus slightly lowering the total efficiency of the array — as can be seen in Fig. 2. A photograph of the nuball/LICORNE coupling is presented on the right of Fig. 5. The black detectors (conical $LaBr_3$ crystals) were retracted to a distance of 10 cm and the grey detectors (cylindrical $LaBr_3$ crystals) were retracted to a distance of 15 cm in order to make sure the source neutrons, produced in a cone of around 20 degrees opening angle, can escape the spectrometer. The experiments using a neutron beam to study the nuclear structure of very neutron-rich fission fragments and the fission mechanism itself, were performed over seven weeks of beam time. The DAQ was run in triggerless mode, and due to the very high count rates and network bandwidth limitations, data were sent to disk at maximum rates of around 70 Mb/s, or 3 Tb per day. The primary beam intensity was set to obtain counting rates in the individual crystals of around 10 kHz in the HPGe, 40 kHz in the BGO and 15 kHz in the $LaBr_3$. The total amount of data collected during the entire ν-ball campaign was very large (~ 0.2 Pb), a significant proportion of which was transferred to the IN2P3 data-center [29].

The last experiment of the campaign replaced all the FATIMA $LaBr_3$ with PARIS phoswitches. A photograph of the coupling is presented in the top panel of Fig. 5. The 34 phoswitches were placed in a cylindrical cluster arrangement at a distance of 20 cm from the center of the array to maximize solid angle coverage. This addition provided a significant increase in the total efficiency at energies greater than 4 MeV. A further 14 FASTER CARAS channels were added to the system, making a total of 200 independent digital channels. This experiment was also run in triggerless mode to allow complete offline characterization of the cross-talk/scattering of γ-rays in the PARIS clusters.

4. Preliminary data analysis

The offline data processing and analysis requires a sequence of steps to reduce the volume of data at each stage.

4.1. File format conversion

The raw data, written on disk by the DAQ system uses a specific binary FASTER format. This format contains extra information about the DAQ status that are irrelevant for data analysis. In addition, in the context of the first four experiments, a trigger condition was set. However, FASTER allows the registration of all the channels that are fired in a time window following a satisfied trigger condition working in a quasi-triggerless mode. Because of timing (see the next item), it has been decided to unfold the trigger structure offline from the registered data. At the same time, a very first step of file conversion to a ROOT format has been created. This procedure keeps all the precise time (down to a value in ps), energy, a FASTER detector label, pile-up information and register it into a ROOT tree. It takes roughly half the acquisition time for a run to be converted to this new data format. In addition, we benefit from the integrated compression of the ROOT format to decrease the amount of required disk space by a factor of three.

4.2. Time calibration and time alignment

When the FASTER cards are initialized, a random delay between channels is generated. This delay comes from the required time for each daughterboard to properly load its configuration. To correct for this random misalignment, and for each reset of the hardware, a specific one-hour calibration run with $^{60}_{27}$Co source had to be performed. In a second step, the time difference distribution between each channel and the reference detector is plotted. The maximum of the coincidence peak position is measured. Then, a time shift is applied to the second detector time stamp to set the coincidence peak absolute position to 0 ns. The result of this procedure is shown in Fig. 6. Each vertical section of a matrix corresponds to a time spectrum of a detector — *w.r.t.* the

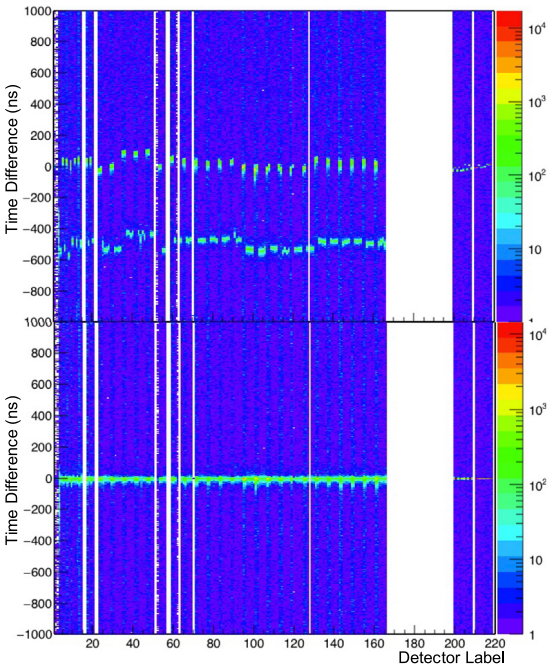

Fig. 6. Time alignment matrix before (on the top) and after (on the bottom) the time correction procedure. For each matrix, the vertical axis represents the time difference between one detector and the reference conical $LaBr_3$ crystal. The horizontal axis represents the detector FASTER label used by the DAQ to recognize each detection channel. The FASTER label below 25 are the Phase I HPGe (even numbers) and their associated BGO (odd numbers). Ranging from 25 to 166 are the 2 Clovers' BGO and the four HPGe crystal (in that order) for each of the 24 clovers. The channels above 199 are, for the first ten the cylindrical $LaBr_3$, and for the last ten, the conical $LaBr_3$ detectors. The vertical stripes represent non-used channel numbers for this specific measurement.

reference $LaBr_3$ which is labeled 210. On the top matrix one can notice how scattered the coincidence peak position can be. Around the 0 ns position, all the detectors that were connected to a CARAS daughter board (BGO and $LaBr_3$) can be found. The others (around −500 ns) corresponds to the MOSAHR daughterboards (HPGe) detectors. One can also notice the asymmetry of the peaks on the matrix. It is mainly due to the low-energy time walk which is caused by the CR-RC4 filter that only simulate a threshold discriminator. From label 200 to 219 the time spectra of $LaBr_3$ are represented. It is easy to differentiate between cylindrical and conical crystals. The later having a better timing resolution, it is visible as the coincidence peak is narrower (see label above 210). The lower matrix represents the position of coincidence peak after timing correction. As intended, all the channels are centered on 0 ns. This correction parameter can remain valid for an entire experiment if no DAQ hardware reset has been performed. In order to finalize the time treatment of the raw data, another time parameter for adjustment is necessary. Indeed, all the experiments used a pulsed beam. The DAQ system registers, in the data stream, a time stamp of one in a thousand pulse from the RF signal that is sent to the beam buncher. Strictly speaking, due to the time-of-flight of the ions, there is a difference of several pulses between the registered one and the effective pulse that can induce a nuclear reaction at the interaction point. But the TOF of the ions vary when the beam tuning is optimized. So, for every run the alignment of the reference detector with the beam pulse is checked and corrected if needed. The same correction has to be propagated to every detectors as they are aligned with this reference $LaBr_3$.

During the timing calibration procedure, the time walk at low energy had to be corrected for. Thanks to the trapezoidal filter of the MOSAHR daughter board and the CFD module attached to the CARAS QDCs, the time walk of HPGe and $LaBr_3$ has been kept below the beam pulse width of 2 ns. However, because of CR-RC4 filter, a coarse (because of their poor energy resolution) time walk correction has been applied to the BGO. After all these modifications, the data need to be arranged by ascending time to optimize the later coincidence reconstruction.

Table 1
Table of the main γ energies used in the calibration process sorted by isotope. Only the absolute γ intensity that have been used for efficiency measurement are indicated.

Isotope	Energy (keV)	Absolute intensity
Th chain	238.63	0.4330
	338.32	0.1127
	463.00	0.0440
	510.77	0.08122
	583.19	0.317
	794.95	0.0425
	911.20	0.258
	2614.51	0.3725
AmBe	59.5	–
	3416.91	–
	3927.91	–
	4438.91	–
Ni(n, γ)	7975	–
	8486	–
	8997	–

4.3. Energy calibration and gain shift tracking

In parallel of timing calibration, an energy calibration of each detector has been performed. Because of their poorer energy resolution, the BGOs were roughly (linear adjustment based on the position of six γ lines) calibrated using ^{137}Cs, ^{241}Am, ^{133}Ba and ^{60}Co standard calibration sources.

The $LaBr_3$ detectors were calibrated using $^{152}_{63}$Eu and ^{nat}Th sources. For the coupling with the PARIS array, higher energy calibration points were needed. An AmBe neutron source was used to induce radiative capture reactions on a Ni foil. The energy of the produced γ-rays are indicated in Table 1. Such a source has been fully characterized in a previous work [30] and produces γ-rays with energy up to 9 MeV. Single and double escape peaks are also used to calibrate. The photomultipliers of some $LaBr_3$ detectors were known not to be linear on the entire energy range. Thus, a second order polynomial was used for a proper calibration of the data.

To obtain the best resolving power from the instrument, the best global energy resolution (after summation of all the detectors together in the analysis), an energy calibration must be performed to the highest possible precision — below 1 keV for HPGe and 10 keV for $LaBr_3$. Non-linearities has to be corrected for. Furthermore, it is important to obtain calibration data over the widest energy range possible to avoid excessive calibration extrapolation. Finally, corrections of gain shifts over time scales of hours, days or weeks must be corrected for. In Table 1, the ^{nat}Th γ-lines used for gain shift tracking and efficiency measurement in the N-SI-109 experiment are shown. In the same table, gamma lines absolute intensities for Th radioactive family are shown.

HPGe detectors are usually very linear over the 0 to 2 MeV energy range. However, a non-linearity can appear due to either the type of HPGe detector (clover or co-axial), a high count rate, or the type of FPGA filter algorithm used (CR-RC4 or Trapezoidal) in the digitizers. Fig. 7 presents the energy difference between the measured energy after the calibration process and the expected value given by the databases for $^{152}_{63}$Eu and the 2.614 MeV γ-line of ^{nat}Th source. One can notice that the non-linearity pattern is different for each detector. Because of its dependance to count rate, it thus has to be tracked and corrected over an hourly time scale. The adopted solution was to use a spline fit between 0.1 and 2.614 MeV. The procedure allowed an improvement of total energy resolution of about .5 keV on the cumulated energy spectrum. This energy resolution gain is illustrated in the bottom part of Fig. 7 that presents the cumulated energy spectrum of all the HPGe

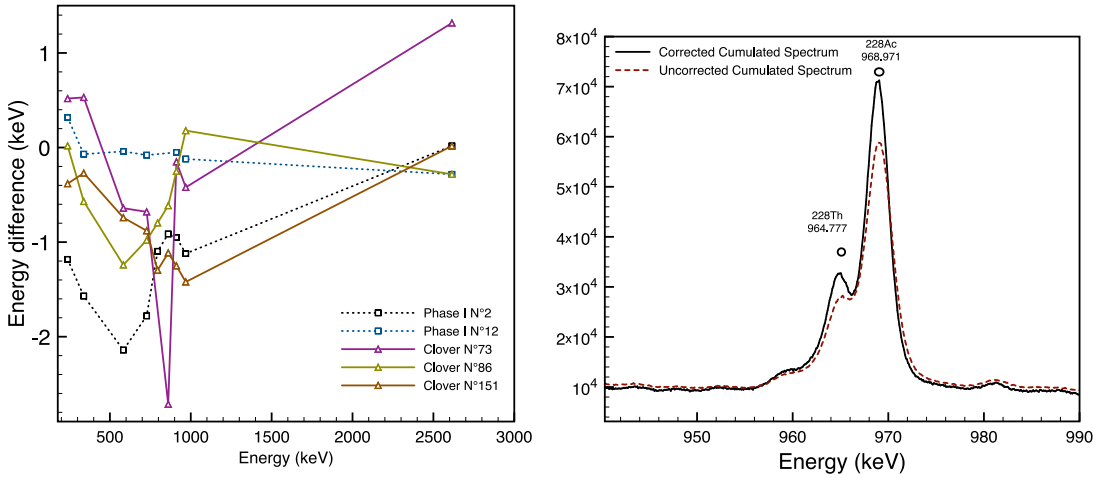

Fig. 7. Top: Energy difference between measured, after the calibration procedure, and expected energy values for $^{152}_{63}$Eu and ^{232}Th sources. The square dashed lines are Phase I HPGe detectors. The triangles represents some Clover crystals. Bottom: Cumulated energy spectrum of all HPGe crystals before and after non-linearity correction. A zoom has been made on a doublet present in the intrinsic activity of the ^{232}Th target that give a visual indication of the energy resolution gain (~ 0.5 keV) thanks to this correction.

crystals before and after the non-linearity correction. A zoom on a doublet (964.78 and 968.97 keV), produced by the intrinsic activity of the target, is shown to illustrate the resolution improvement. After this procedure, data file containing sorted time aligned and energy calibrated ROOT trees were produced.

4.4. Reaction calorimetry with ν-ball

From these new files, the event building for each experiment can be adapted for optimal selection. However, the global analysis procedure has the common characteristic of determination of the relative position in time of prompt gamma rays coincident with the beam pulsation (400 ns period) and the corresponding determination of prompt γ multiplicity and sum energy.

Fig. 8 shows an example of ν-ball calorimetry for the $^{18}_{8}$O + $^{164}_{66}$Dy heavy ion reaction near the Coulomb barrier. The prominent exit channels are Coulomb excitation of the target ^{164}Dy, two nucleon transfer ^{164}Dy(^{18}O,^{16}O)^{166}Dy and fusion-evaporation ^{164}Dy(^{18}O,2n)^{178}Hf. Since each reaction has a very different multiplicity and sum-energy distribution, preferential channel selection can easily be achieved by setting different gates on the multiplicity, M_γ (k), and sum energy, E_{tot} (H).

An horizontal cut has been performed. On the left part, two spectra are presented. The one on the bottom, corresponding to low total energy clearly display the sequence of γ lines produced in the Coulomb excitation of the ^{164}Dy target. On the contrary, the upper spectrum, corresponding to a higher total measured energy cut presents the γ line of nuclei produced in the fusion-evaporation mechanism.

The selectivity of the calorimetry can clearly be seen in the two different gamma spectra. Fig. 8 shows the functioning of the calorimetry from the opposite point of view, where we determine the process occurring either due to the detection of a $^{252}_{98}$Cf spontaneous fission (SF) fission fragment, or a β-decay event. In the context of fission, the average γ-ray multiplicity emitted is around 8 γ/fission and a total energy of about 6 MeV [30] (see Fig. 9).This can be compared to the typical $^{152}_{63}$Eu β decay multiplicity ($2-3\gamma$/decay) or the (n,n′γ), (n, γ) reactions ($1-2\gamma$/reaction) and the total energy of the same processes (Q_β values for close to stability nuclei and/or incident neutron energy of about 2 MeV). Based on these values, one can imagine two specific regions in the Hk matrix corresponding to the fission and to the parasitic processes with of course some overlap. For this reason, the calorimetry alone might not be a stringent enough trigger condition to reconstruct all the fission events. Some more evolved trigger conditions based on fuzzy logic [31,32] are now being studied to improve the fission event reconstruction.

5. Conclusion

From November 2017 to June 2018, the ALTO facility of the Institut de Physique Nucléaire d'Orsay hosted an experimental campaign with the ν-ball spectrometer. The innovative features of this device are: hybrid detector setup allowing fast timing, fully digital DAQ allowing calorimetry for reaction selection/measurement, and coupling with the LICORNE directional neutron source to facilitate precision spectroscopy of neutron induced reactions. It was also the first fully digital large fast timing setup with time resolutions comparable to analogue CFD/TAC electronics. In a very tight schedule (about one year): detectors were delivered to Orsay, where they were tested, mounted, and commissioned. Eight experiments were performed. Preliminary data analysis confirms the expected performances of the ν-ball array. Data analysis procedures (e.g. calibration, gain tracking, time alignments) have been defined to ensure optimal data quality, including definition of prompt γ-ray event detection and the associated multiplicity and sum energy for both triggered and triggerless data. The ν-ball campaign has thus been demonstrated as a technical success, despite the time constraints.

Declaration of competing interest

The authors declare that they have no known competing financial interests or personal relationships that could have appeared to influence the work reported in this paper.

CRediT authorship contribution statement

M. Lebois: Conceptualization, Methodology, Software, Validation, Formal analysis, Investigation, Resources, Data curation, Writing - original draft, Writing - review & editing, Visualization, Supervision, Project administration, Funding acquisition. **N. Jovančević:** Methodology, Software, Validation, Formal analysis, Investigation, Resources. **D. Thisse:** Methodology, Software, Validation, Formal analysis, Investigation, Resources. **R. Canavan:** Methodology, Software, Validation, Formal analysis, Investigation, Resources. **D. Étasse:** Methodology, Software, Validation, Resources. **M. Rudigier:** Methodology, Software, Validation, Formal analysis, Investigation, Resources. **J.N. Wilson:** Conceptualization, Methodology, Software, Validation, Formal analysis, Investigation, Writing - original draft, Supervision, Project administration, Funding acquisition.

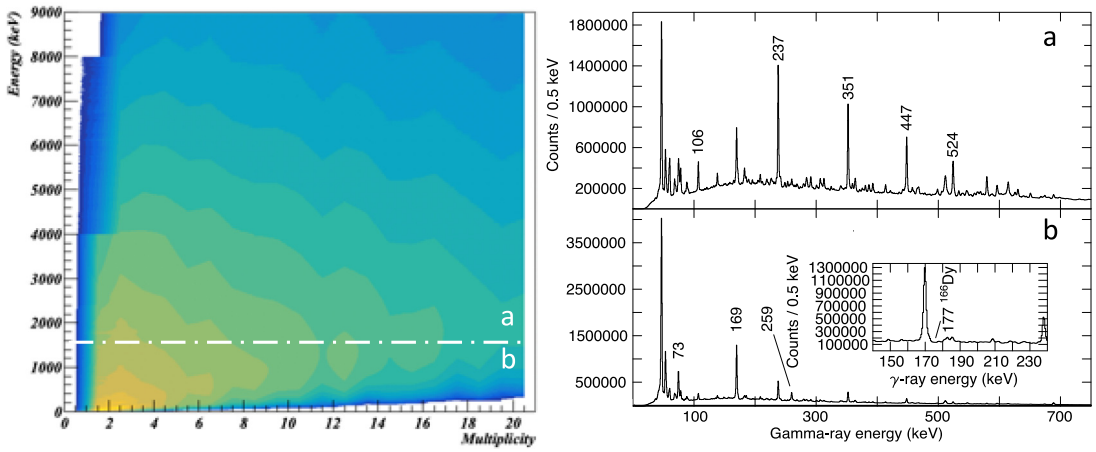

Fig. 8. In the center, total energy *vs.* modular multiplicity matrices (Hk matrix). On the right, it corresponds to the γ spectra created by selecting region a or b of the Hk matrix.

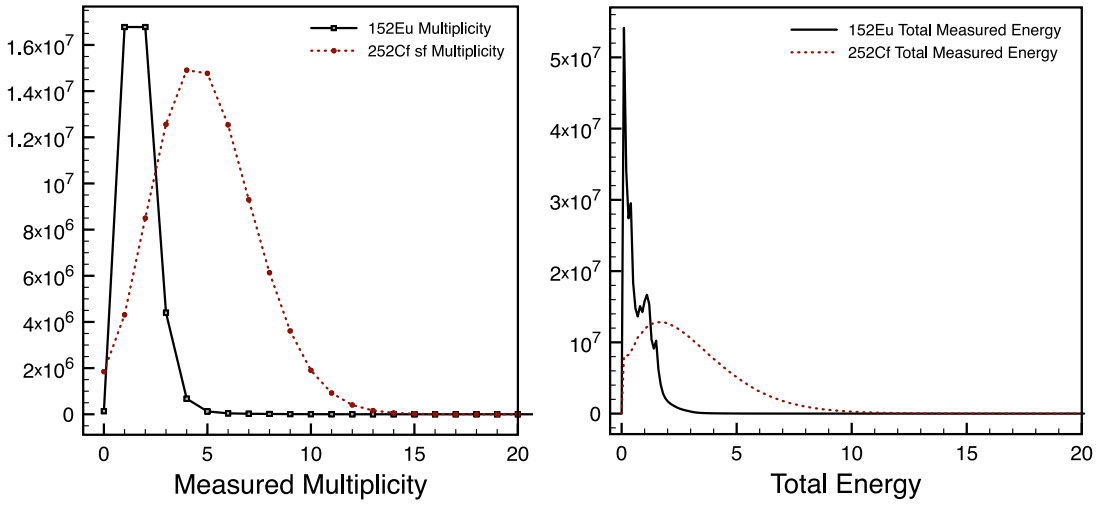

Fig. 9. Comparison of Total Sum Energy and multiplicity detected inside ν-ball for tagged 252Cf spontaneous fission events, and events from the beta-decay of 152Eu.

Acknowledgments

We would like to thank the operators of the ALTO facility for providing us with reliable beams used in the experiments. We would like to express our profound gratitude to the FASTER collaboration for their strong technical support over the course of the campaign. We would like to acknowledge the support of the GAMMA-POOL and the LOANPOOL for the loan of the Clovers and Phase I germanium detector. We also acknowledge the FATIMA and the PARIS collaborations for the loan of their $LaBr_3$ crystals and PARIS phoswitches. The research leading to these results has received funding from the European Union's HORIZON2020 Program under grant agreement n° 654002.

References

[1] U. F. E. Collaboration, Nuclear Phys. A 520 (1990) c657 – c667.
[2] J. Eberth, et al., Prog. Part. Nucl. Phys. 28 (1992) 495–504.
[3] F.A. Beck, Prog. Part. Nucl. Phys. 28 (1992) 443–461.
[4] I.-Y. Lee, Nuclear Phys. A 520 (1990) c641–c655.
[5] C. Sotty, AIP Conf. Proc. 1852 (2017) 080009.
[6] V. Werner, et al., J. Phys.: Conf. Ser. 366 (2012) 012048.
[7] K.S. Shah, et al., IEEE Trans. Nucl. Sci. LBNL-51793 (2002).
[8] V. Vedia, et al., Nucl. Instrum. Methods A 857 (2017) 98–105.
[9] D. Bucurescu, et al., Nucl. Instrum. Methods Phys. Res. A 837 (2016) 1–10.
[10] M. Rudigier, et al., Acta Phys. Polon. B 50 (3) (2019).
[11] S. Leoni, et al., Acta Phys. Polon. B 50 (3) (2019).
[12] N. Jovancevic, et al., Acta Phys. Polon. B 50 (3) (2019).
[13] M. Lebois, et al., Nucl. Instrum. Methods A A (735) (2014) 145.
[14] http://gammapool.lnl.infn.it/index.htm.
[15] A. Maj, et al., Acta Phys. Polon. B 40 (3) (2009) 565–575.
[16] M. Zieblinski, et al., Acta Phys. Polon. B 44 (2013) p. 651.
[17] C. Ghosh, et al., J. Instrum. 11 (5) (2016) P05023.
[18] J. Allison, et al., Nucl. Instrum. Methods A 506 (2003) 250.
[19] http://ipnwww.in2p3.fr/GePool/poolRules.html.
[20] O.J. Roberts, et al., Nucl. Instrum. Methods A 748 (2014) 91–95.
[21] http://www.ukndn.ac.uk.
[22] http://faster.in2p3.fr.
[23] R. Brun, F. Rademakers, Nucl. Instrum. Methods Phys. Res. A 389 (1997) 81–86.
[24] R.D.G. Sarantites, R. Woodward, Nucl. Instrum. Methods 171 (3) (1980) 503–519.
[25] R. Simon, J. Phys. Colloq. 41 (1980) 281–293.
[26] J. Martin, et al., Nucl. Instrum. Methods A 257 (1987) 301–308.
[27] M. Jandel, et al., Physics Procedia 59 (2014) 101–106.
[28] M. Lebois, et al., Acta Phys. Polon. B 50 (3) (2019).
[29] https://cc.in2p3.fr/en/.
[30] L. Qi, et al., Statistical study of the prompt-fission γ-ray spectrum for ^{238}u(n,f) in the fast-neutron region, Phys. Rev. C 98 (2018) 014612.
[31] B. Kosko, The Fuzzy Future, Harmony Books, 1999.
[32] B. Kosko, Fuzzy Thinking: The New Science of Fuzzy Logic, Hyperion, 1993.